Computational and Experimental Study of a Microwave Electromagnetic Bandgap Structure With Waveguiding Defect for Potential Use as a Bandpass Wireless Interconnect

J. J. Simpson, *Student Member, IEEE*, A. Taflove, *Fellow, IEEE*, J. A. Mix, and H. Heck

***Abstract*—As clock rates continue to rise, problems with signal integrity, cross-coupling, and radiation may render impractical the baseband metallic interconnects presently used in computers. A potential means to address this problem is to use bandpass wireless interconnects operating at millimeter-wave center frequencies. We have conducted experimental and finite-difference time-domain (FDTD) computational studies scaled to a 10 GHz center frequency of single-row and double-row waveguiding defects within an electromagnetic bandgap structure. Our initial experimental results scaled to 10 GHz have verified the feasibility of achieving an approximately 80% bandwidth with excellent stopband, gain flatness, and matching characteristics. When scaled to millimeter-wave center frequencies above 300 GHz, this technology appears feasible of supporting data rates in the hundreds of Gb/s.**

***Index Terms*—Finite-difference time-domain (FDTD), metallic electromagnetic bandgap (EBG) structure, millimeter wave, waveguide, wireless interconnects.**

I. Introduction

SINCE their inception, computers have been constructed using baseband metallic interconnects to transfer data between processors. However, much above the present clock rates of about 3 GHz, problems with signal integrity, cross-coupling, and radiation may render this type of interconnect impractical. Since clock rates approaching microwave frequencies of 20 GHz are projected by 2010, attention is being drawn toward alternative technologies that have relatively favorable signal transmission characteristics. While optical interconnects could easily provide the necessary bandwidth, there are major difficulties in integrating the required GaAs laser sources into existing silicon chip technology.

We are investigating an alternate possibility, using bandpass wireless interconnects at millimeter-wave frequencies. Such an approach could take advantage of emerging terahertz (THz) silicon transistor technology [1]. This letter reports a computational and experimental study of a promising waveguiding structure for such interconnects: linear defects in periodic electromagnetic bandgap (EBG) structures [2]–[6]. Our initial experimental results scaled to 10 GHz have verified the feasibility of achieving an approximately 80% bandwidth with excellent stopband, gain flatness, and matching characteristics.

Manuscript received December 3, 2003; revised March 9, 2004. This work was supported by Intel Corporation and the Pittsburgh Supercomputing Center under Grant ECS020006P. The review of this letter was arranged by Associate Editor J.-G. Ma.

J. J. Simpson and A. Taflove are with the Electrical and Computer Engineering Department, The Technological Institute, Northwestern University, Evanston, IL 60208-3118 USA.

J. A. Mix and H. Heck are with Interconnect Technologies, Intel Corporation, Hillsboro, OR 97124 USA.

Digital Object Identifier 10.1109/LMWC.2004.829283

II. Computational Modeling Technique

In all of our simulations, we have employed the standard FDTD method implemented on a uniform 2-D Cartesian grid [7] using a space-cell size of 0.48 × 0.48 mm. This cell size has been found to yield numerically converged results relative to rendering the geometry of the array of metal pins comprising the EBG structure. Because each grid cell spans at most about 1/70th wavelength in the direction of propagation at 10 GHz (the approximate center of the waveguiding passband of interest), numerical phase velocity errors are in the order of 1.7×10^{-4} [7].

Relative to our study of pure monomodal propagation in Section IV, we elongated the FDTD waveguide model in the direction of propagation to permit evanescent numerical modes generated at the source plane to fully decay. Subsequently, all numerical calculations of modal propagation in Section IV were conducted in the waveguide region where the modal distribution completely stabilized. We also used the technique described in [8] wherein the FDTD model of the EBG waveguide is simply continued for a sufficient distance into a perfectly matched layer (PML) absorbing boundary. This yields reflection errors of less than 10^{-4}.

III. Computation of the Stopband of the Defect-Free 2-D EBG Structure

We first report our application of FDTD modeling to calculate the stopband of the defect-free EBG structure for the E-polarization case (electric field parallel to the pins). The EBG structure is comprised of a square arrangement of copper pins of radius r in air with a uniform center-to-center spacing of a. The inset of Fig. 1 shows the unit cell for the EBG structure and its associated periodic boundary conditions [7].

Our numerical experiments involved numerous FDTD simulations of impulsive electromagnetic field transmission through the EBG structure for a normally incident, E-polarized plane wave. This tested a variety of combinations of r and a to obtain approximately the optimum values for stopband width and waveguide transmission. Results are obtained for the magnitude

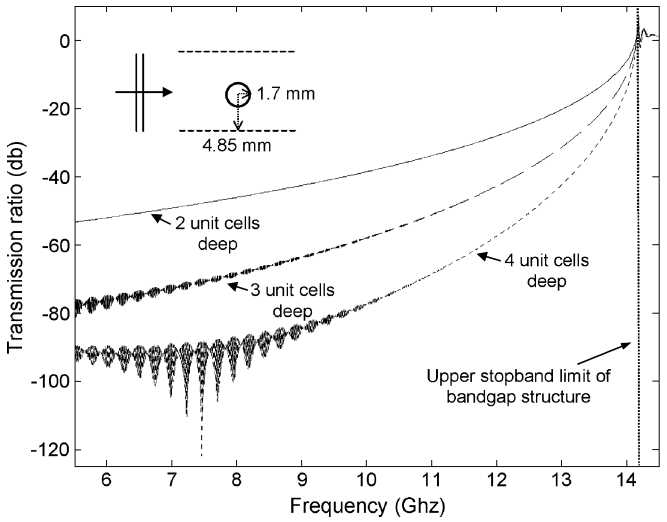

Fig. 1. FDTD-calculated magnitude (E-polarization case) of the electric-field transmission transfer function through the first two, three, and four unit cells of a 2-D square arrangement of metal pins having $r = 1.7\ \mathrm{mm}$ and $a = 9.7\ \mathrm{mm}$.

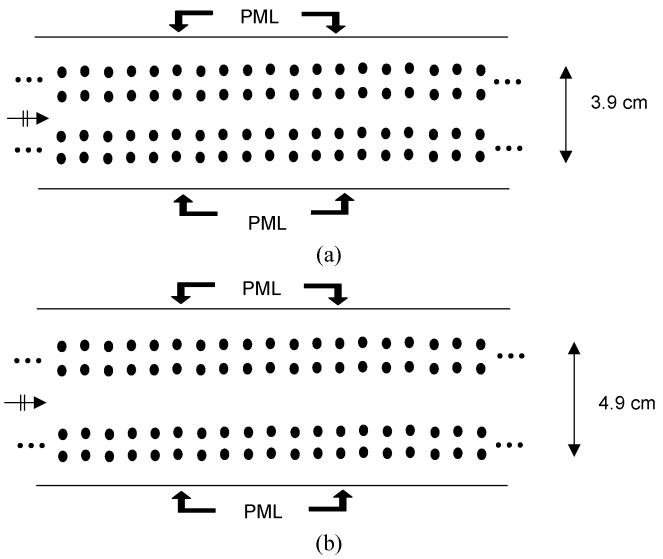

Fig. 2. Waveguiding defects embedded within the square EBG structure of metal pins of Fig. 1. (a) Single-row defect created by removing one row of pins from a structure having initially five rows of pins and (b) double-row defect created by removing two rows of pins from a structure having initially six rows of pins.

of the E-field transmission as a function of frequency at various depths into the structure for:

1) surface impedance $\mathrm{Z_s} = 0$;
2) frequency-independent $\mathrm{Z_s}$ set to that of copper at approximately 10 GHz [7].

Negligible differences are observed between these two cases for a center frequency of 10 GHz, so for our subsequent studies in this work we assumed $\mathrm{Z_s} = 0$.

Fig. 1 shows the EBG structure stopband observed two, three, and four unit cells deep for the nearly optimum case $r = 1.7\,\mathrm{mm}$ and $a = 9.7\,\mathrm{mm}$. Here, the stopband is seen to extend from dc to approximately 14.1 GHz. In our subsequent discussion, we shall take 14.1 GHz as the upper limit of the permissible passband of the EBG structure with waveguiding defect, since above that frequency field confinement is lost.

IV. Computation of the Passband of the 2-D Waveguiding Defect

Fig. 2(a) illustrates the geometry of a single-row waveguiding defect created by deleting one row of pins from an approximately optimum 2-D EBG structure in air (see Section III) having initially five unit cells (as defined in Fig. 1 and Section III) in the lateral direction. The overall lateral dimension of this waveguide structure is 3.9 cm. Fig. 2(b) illustrates the geometry of a double-row waveguiding defect created by deleting two rows of pins from an approximately optimum 2-D EBG structure having initially six unit cells in the lateral direction. The overall lateral dimension of this waveguide structure is 4.9 cm.

Upon implementing the methodology to generate a pure mode discussed in Section II, we applied 2-D FDTD modeling to calculate for each waveguiding defect the magnitude and phase of the electric field transmission characteristic over a 45-cm longitudinal span along the center axis of the waveguide. Defining the usable transmission bandwidth as the frequency span over which the transmission magnitude variations are less than ± 1 dB, the transmission bandwidth for the single-row waveguiding defect is calculated to be 55% (6.1 GHz) centered about 10 GHz, and 85% (8.7 GHz) for the double-row waveguiding defect. Further analysis indicates that the phase of the electric field transmission characteristic corresponding to the single-row waveguiding defect is linear to within $\pm 1.8^\circ/\mathrm{GHz}$ over the full passband, and to within $\pm 1.1^\circ/\mathrm{GHz}$ for the double-row waveguiding defect. The latter is therefore preferable from the standpoint of bandwidth and phase linearity.

To examine the possibility of multimoding [6], we performed numerical experiments that offset the source distribution in the transverse direction. These experiments indicated little (if any) evidence of odd-mode generation.

V. Computational and Laboratory Experiments

Following the design guidelines established by the 2-D FDTD modeling discussed in Section IV, we conducted 3-D FDTD modeling and laboratory measurements of prototype microwave EBG waveguiding structures with linear double-row defects. These structures were realized using double-sided circuit board having standard FR4 as the dielectric material ($\text{approximate relative permittivity} = 4.3$ and $\text{loss tangent} = 0.017$). Copper vias electrically bonded to the upper and lower ground planes served to implement the rows of EBG pins. In each case, the waveguiding structures were dimensionally scaled to operate at a 10-GHz center frequency. The structures were coupled to input and output coaxial lines via short probes extending transversely across the gap between the upper and lower ground planes and bonded to the opposing ground plane.

Fig. 3 is a photo of one of the test structures. This structure spans 10 cm between the input and output probes; 3.2 mm between the upper and lower ground planes; and 13.8 mm (center-to-center) between the rows of vias immediately bounding the waveguiding defect. A second structure, identical to that shown in Fig. 3 but spanning 6 cm between the input and output probes, was also constructed to permit isolation of the effect of the dielectric loss of the FR4. Because the radius and spacing of the copper pins scales relative to the dielectric

Fig. 3. Test structure comprised of FR4 circuit board (relative permittivity $= 4.3$ and loss tangent $= 0.017$) with the transmit and receive probes (50-Ω nominal source and load impedances) bonded to the opposing ground plane. This structure spans 10 cm between the input and output probes; 3.2 mm between the upper and lower ground planes; and 13.8 mm (center-to-center) between the rows of vias immediately bounding the waveguiding defect. The radius and spacing of the vias are $r = 0.83\,\mathrm{mm}$ and $a = 4.6\,\mathrm{mm}$, respectively.

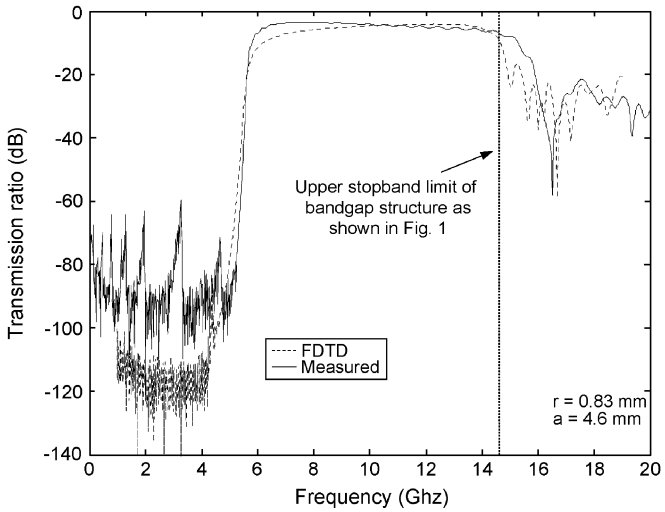

Fig. 4. Comparison of FDTD-calculated and measured results for the insertion loss of the FR4 double-row defect shown in Fig. 3. The upper stopband limit of the EBG structure of Fig. 1 is also shown. The measured insertion loss over the passband from 6 to 14.1 GHz ranges from 3.6–7.3 dB with an average of 4.6 dB. In comparison, the FDTD-calculated insertion loss over the same frequency band ranges from 4.2–9.5 dB with an average of 5.3 dB.

constant of the material between the pins, the pins of these test structures have $r = 0.83\,\mathrm{mm}$ and $a = 4.6\,\mathrm{mm}$. Note that the waveguiding defect is bounded on all sides by the EBG structure, thereby representing effectively a closed cavity (leakage below -40 dB at 10 GHz predicted by the FDTD model, as shown in Fig. 1).

Fig. 4 compares FDTD-calculated and measured results for the insertion loss of the 10-cm-long FR4 double-row defect shown in Fig. 3. A standard 20-GHz Agilent microwave network analyzer having 50-Ω nominal source and load impedances was used in these measurements. From Fig. 4, we see that there exists a sharp transition in the measurement results from a stopband of -80 dB to a passband at approximately 6 GHz. The measured insertion loss over the passband from 6 to 14.1 GHz (the upper stopband limit of the bandgap as shown in Fig. 1) ranges from 3.6 to 7.3 dB with an average of 4.6 dB. In comparison, the FDTD-calculated insertion loss over the same frequency band ranges from 4.2 to 9.5 dB with an average of 5.3 dB. These results support our basic concept that an 80% fractional bandwidth is feasible using double-row defect EBG structures [9].

Fig. 4 shows that the total insertion loss at midband (10 GHz) of the 10-cm-long waveguiding defect is 4.2 dB. Comparison of this result with that of the 6-cm-long waveguiding defect indicates that 3.5 dB of the 4.2 dB total loss is introduced by the propagation attenuation caused by the FR4 dielectric. Subtracting the FR4 dielectric loss from the total insertion loss, our data indicates a total input/output coupling loss of only 0.7 dB at the coaxial transitions on either end of the waveguiding channel. This indicates the possibility of excellent broadband matching into the waveguiding defect.

Migration of this technology to the millimeter-wave regime appears feasible. A primary requirement is the use of dielectric materials having low loss up to several hundreds of GHz. Candidate materials for this application include aerogels [10]. On the FDTD modeling side, it will be important to properly model the frequency-dispersive dielectric properties of the metal pins. Here, either a dispersive surface impedance model [11] or a bulk-Drude model [12] might be applied.

VI. Conclusion

We have performed a computational and experimental study of a promising new wireless interconnect technology for high-speed digital circuits employing linear defects in electromagnetic bandgap structures. Our initial experimental results scaled to 10 GHz have verified the feasibility of achieving an approximately 80% bandwidth with excellent stopband, gain flatness, and matching characteristics. When scaled to millimeter-wave center frequencies above 300 GHz (to leverage emerging silicon transistor technology), the wireless interconnects reported in this letter should be feasible of supporting data rates in the hundreds of Gb/s, assuming the availability of suitable low-loss dielectrics.

References

[1] R. F. Service, "World's smallest transistor," *Science*, vol. 293, p. 786, Aug. 3, 2001.
[2] E. Yablonovitch, "Photonic band-gap structures," *J. Optical Soc. Amer. B*, vol. 10, pp. 283–295, 1993.
[3] J. D. Joannopoulos, R. D. Mead, and J. N. Winn, *Bandgap Structures: Molding the Flow of Light*. Princeton, NJ: Princeton Univ. Press, 1995.
[4] A. Mekis, S. Fan, and J. D. Joannopoulos, "Bound states in bandgap structure waveguides and waveguide bends," *Phys. Rev. B*, pp. 4809–4817, 1998.
[5] M. Thevenot, A. Reineix, and B. Jecko, "FDTD approach for modeling PBG structures," *J. Opt. Soc. A: Pure Appl. Opt. 1*, pp. 495–500, 1999.
[6] M. Qiu and S. He, "Guided mode in a two-dimensional metallic bandgap structure waveguide," *Phys. Lett. A*, pp. 425–429, 2000.
[7] A. Taflove and S. C. Hagness, *Computational Electrodynamics: The Finite-Difference Time-Domain Method*, 2nd ed. Norwood, MA: Artech House, 2000.
[8] M. Koshiba, Y. Tsuji, and S. Sasaki, "High-performance absorbing boundary conditions for bandgap structure waveguide simulations," *IEEE Microwave Wireless Comp. Lett.*, vol. 11, pp. 152–514, Apr. 2001.
[9] L. Couch III, *Digital and Analog Communication Systems*, 5th ed. Upper Saddle River, NJ: Prentice-Hall, 1997.
[10] S.-K. Fan, J.-A. Paik, P. Patterson, M. C. Wu, B. Dunn, and C.-J. Kim, "MEMS with thin-film aerogel," in *Proc. IEEE Conf. Micro Electro Mechanical Systems (MEMS'01)*, Interlaken, Switzerland, Jan. 2001, pp. 122–125.
[11] J. G. Maloney and G. S. Smith, "The use of surface impedance concepts in the finite-difference time-domain method," *IEEE Trans. Antennas Propagat.*, vol. 40, pp. 38–48, 1992.
[12] J. T. Krug II, E. J. Sanchez, and X. S. Xie, "Design of near-field optical probes with optional enhancement by finite-difference time-domain electromagnetic simulation," *J. Chem. Phys.*, vol. 116, no. 24, pp. 10 895–10 901, June 2002.